Theor Chem Acc (2015) 134:147
DOI 10.1007/s00214-015-1750-3

REGULAR ARTICLE

Helical molecular redox actuators with pancake bonds?

Pierre Beaujean[1,2] · **Miklos Kertesz**[2]

Received: 23 July 2015 / Accepted: 22 October 2015

Abstract In an attempt to design molecular electromechanical actuators with large deformation response, we present here three helicene-like compounds, which offer significant strain above 5 % due to two-electron charge transfer (CT). The shrinking induced by CT is a quantum mechanical orbital effect. A good π–π overlap across the helical pitch is critical for this type of actuation. The relevant overlap refers to frontier orbitals that are involved in the CT, and it has some features common with π–π stacking pancake bonds; however, these molecules do not represent all aspects of typical pancake bonding. This overlap is accompanied by a change in the bond length alternation pattern indicating significant change in π-conjugation. Additionally, two further helicene-like molecules included in this study also indicate large electromechanical actuation, but a simple orbital interpretation is not available in those cases.

Keywords Molecular actuators · Charge transfer · Helical structure · π–π Overlap · Density functional theory computations

Published as part of the special collection of articles "Festschrift in honour of P. R. Surjan".

Electronic supplementary material The online version of this article (doi:10.1007/s00214-015-1750-3) contains supplementary material, which is available to authorized users.

✉ Miklos Kertesz
kertesz@georgetown.edu

[1] Laboratoire de Chimie Théorique, Unité de Chimie Physique Théorique et Structurale, Université de Namur, rue de Bruxelles 61, 5000 Namur, Belgium

[2] Department of Chemistry and Institute of Soft Matter, Georgetown University, 37th and O Streets, NW, Washington, DC 20057-1227, USA

1 Introduction

Molecular actuators present large and reversible structural changes triggered by an external stimulus [1, 2]. The potential applications of such systems range from molecular electronics to nanotechnology [3, 4]. Actuation mechanism is based on the ability of the system to transform this external stimulus into mechanical work. The signal can take many forms: optical [5], chemical, or electrical [6], which allows a wide range of systems to be used, such as synthetic foldamers [7–9] or functional molecular rotaxanes [10, 11]. The review by Baughman et al. [1] summarized various advantages and limitations of those systems.

In particular, the external stimuli can be a consequence of chemical or electrochemical doping, for example in the case of conducting polymers (polypyrroles [12, 13], polyanilines [14, 15] or polythiophenes [16]) or single-walled carbon nanotubes [17]. Electromechanical actuators, in which the conformational or configurational change is caused by a redox event, have attracted significant attention [18–21]. This class also includes, for example, redox-controlled S···N interactions [22] and π-dimers formation [23–25]. In these cases, the redox event triggers a modification of the frontier orbital pattern which is a quantum mechanical (QM) orbital effect. The overlap of the singly occupied molecular orbitals (SOMOs) creates multicenter/2-electron bonds (mc/2e), which are generally found in π-radical dimers, where they are called *pancake* bonds [26–33]. These multicenter π-stacking bonds present a number of unusual characteristics, one being that the contact distances are shorter than the classical van der Waals (vdW) distances [34]. They also present some characteristics of covalent bonds: These bonds are typically significantly stronger than vdW contacts and have ESR-silent diamagnetic character providing evidence for

Published online: 12 November 2015

electron pairing [35]. Those observations are coherent with the molecular orbital description of the phenomenon, where two singly occupied molecular orbitals (SOMOs) overlap to form a bonding inter-molecular orbital between the two molecules, like the electron pair in a covalent bond (Fig. 1), in a *trough space* fashion across the vdW separation. However, those bonds are much weaker than conventional bonds and are longer than covalent ones (for example, the CC covalent distance is 1.54 Å, while pancake bonds are around 3.1 Å). They also often retain a diradicaloid character [35].

Combining these two concepts, it may be interesting to look into highly π-conjugated molecules for intramolecular orbital interactions with significant overlap across the vdW separation triggered by a redox charge transfer (CT) process. The candidates must present possibilities of π–π stacking, and therefore, aromatic helical molecules are very appealing. In the past, helical structures were already envisaged for molecular actuation, for example helicene [36] and *o*-phenylene [37–39]. The helical architecture is attractive because the helical molecule holds the π-electron network in place and is ready made for through space bonding and antibonding interactions that is then exploited for redox actuation. The critical question is whether for any given helix, there is sufficient frontier orbital overlap matching across the pitch. Given the subtle dependency of this overlap as a function of the molecular architecture, only computations at the appropriate level can help select systems for this goal.

In this paper, we will present computational results for helicene-like molecules testing the idea whether such an architecture could be exploited for molecular redox actuation using the π–π overlap across the space of the helical pitch. We selected systems from components for which crystal structures have been reported in the literature (Fig. 2).

A quantitative measure of a molecular actuator is the magnitude of geometrical change as function of the amount and sign of the charge transferred to the molecule, q, in terms of the number of electrons added ($X^{|q|-}$, reduction) or removed ($X^{|q|+}$, oxidation), and the following formula can be used to characterize them:

$$s(q) = \frac{\Delta l(q)}{l} \times 100\,\% \tag{1}$$

where s is the (linear) strain, defined as the ratio of the change $\left[\Delta l = l(q) - l(0)\right]$ to the length (l) in a given direction [42]. Addition or removal of electrons leads normally to Coulombic repulsion ($\propto 1/r$, where r is the distance between two charges), and therefore, for most systems, this strain is positive. We will then show that the systems listed in Fig. 2 display significant s values for at least one direction of CT, which can be used to design molecular actuators triggered by redox processes with strain values comparable to those obtained previously for other systems [1].

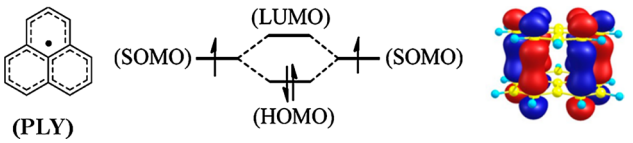

Fig. 1 Orbital interaction diagram between two π-radicals, example of the phenalenyl (PLY) with the representation of the HOMO with strong bonding interaction across the vdW separation in the dimer [35]

2 Computational methodology

In this paper, we will focus on molecules **1b**, **2b**, and **3**. **1b** was chosen instead of **1a**, for which the methyl units can cause steric hindrance, and **2b** is longer than the experimentally available **2a** presenting a minimal length so that at least part of the molecule overlaps with another part of the molecule in a π–π stacking fashion. All structures were

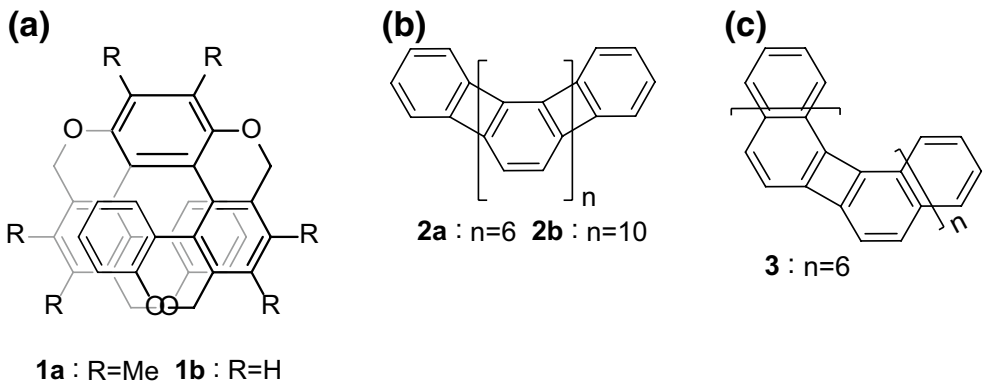

Fig. 2 Structures of the helicene-like molecules: **a** sketch of helicene incorporating saturated sp^3 carbons, distorted metric shows connectivity (**1a** from Kimura et al. [40]). **b** Heliphene (**2a** from Han et al. [41]) and **c** heliphene with naphthalene units

optimized using density functional theory at the UM05-2X/6-31G(d,p) level, for charges going from +2 to −2, except for **2b**, which was optimized at the (R)M05-2X/6-31G(d,p) level. The M05-2X functional is a hybrid functional with 52 % of Hartree–Fock exchange [43], which was previously found to give accurate results for conjugated systems with pancake bonds [44]. We found that the restricted and unrestricted levels give geometries in close agreements with each other. We obtained zero spin densities in all cases when there was a good overlap across the helical pitch. For this reason, calculations at the unrestricted level provided no new information. The structures present a C_2 symmetry, except for $\mathbf{1b}^{2+}$. All calculations were performed using the Gaussian 09 package [45]. We used the graphics program ChemCraft [46].

To characterize such structures, we have used three different approaches which are listed below. The Cartesian coordinates (x, y, z) of the ith atom of a helix are given by the parametric Eq. (2),

$$\begin{cases} x_i = r_i \cos\theta_i \\ y_i = r_i \sin\theta_i \\ z_i = \dfrac{p_i}{2\pi}\theta_i \end{cases} \tag{2}$$

where θ_i is the angle (in radian), r_i is the radius (in Å), and p_i the pitch (in Å) of the helix (width of one complete helical turn, measured parallel to the axis of the helix along the axis, Fig. 3) [47].

Many helical molecules lack perfect "helical staircases" in which repeat units would be perpendicular to the helical axis making it necessary to define an average pitch value. Due to this and due to end effects, we used three alternative measures for the change of the pitch and l: $\bar{p}$, Δz, and $\overline{d_{CC}}$, as defined below. These are based on the atomic numbering for the carbon atoms located in the inner part of the helices (Figs. 4, 5, 6), because we found that those carbons showed the largest changes in contact distances as they respond to CT. Note that the two first and last carbons of **2b** and **3** are not considered, because the terminal regions deviate most from the helical symmetry.

The three measures used for the quantitative description of the changes of the helical geometry are $\bar{p}$, Δz, and $\overline{d_{CC}}$, and they are defined below. The following algorithm was used to obtain average pitch, $\bar{p}$. First, we used Eq. (2) in order to find r_i, θ_i, and p_i for each carbon in each molecular (repeat) units; their indices are listed in Table 1. Then, the average radius, $\bar{r}$, is retrieved from the average of all r_i values. $\bar{p}$ is calculated by taking the slope (and forcing the trend line to pass through zero) of the graph of z_i with respect to θ_i. The reason for choosing this algorithm is that we observed that directly averaging p_i leads to a strong dependency on the choice of the Z axis for the molecule producing large standard deviations. In this paper, the Z axis is chosen by taking

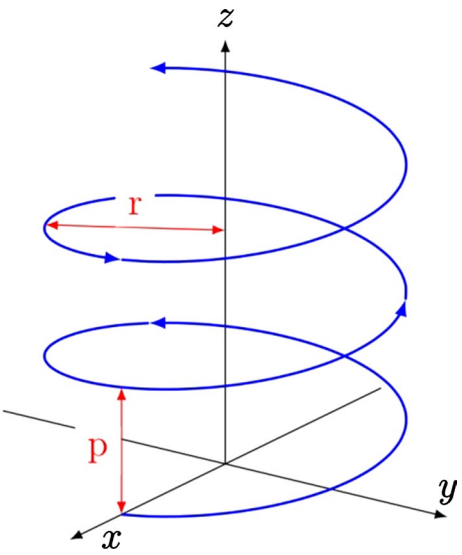

Fig. 3 Definition of the helical axis and parameters, with r the radius and p the pitch

the mean vector that passes through the centers of the circles determined for each consecutive three carbons listed in Table 1. $\bar{p}$ and $\bar{r}$ give therefore quantitative measures of the global conformational changes induced by CT.

Another metric is Δz, the difference in the z coordinates of the first and the last atom considered in the previous process (bold indices in Table 1). Finally, since the lowest intramolecular C···C through space contact distances across the pitch were found to be on the inner part of the molecules, the shortest C···C distances, d_{CC}, were measured, by taking the three shortest contacts for each inner atom (Table S1). An average of these three values, $\overline{d_{CC}}$, was then be evaluated, giving an insight into the overall length change of the molecule. This value should correlate with the average pitch, $\bar{p}$.

To validate this analysis, an error was estimated by measuring the average deviation from helicity, $\bar{D}$, between the coordinates of the carbon in the structure $(x_{C,i}, y_{C,i}, z_{C,i})$ and the one obtained by using Eq. (2) with our $\bar{r}$ and $\bar{p}$, which is the position if the structure was a "perfect helix" (x_i, y_i, z_i):

$$\bar{D} = \frac{1}{N}\sum_{i}^{N} D_i \quad \text{with}$$
$$D_i = \sqrt{\left(x_i - x_{C,i}\right)^2 + \left(y_i - y_{C,i}\right)^2 + \left(z_i - z_{C,i}\right)^2}. \tag{3}$$

$\bar{D}$ is zero if the structure is a perfect helix, and $\bar{r}$ and $\bar{p}$ fit perfectly, and a large value means structure deviates significantly from a helix.

To characterize the optimized structures, another structural parameter was also used: the bond length alternation (BLA), defined as the mean difference between the

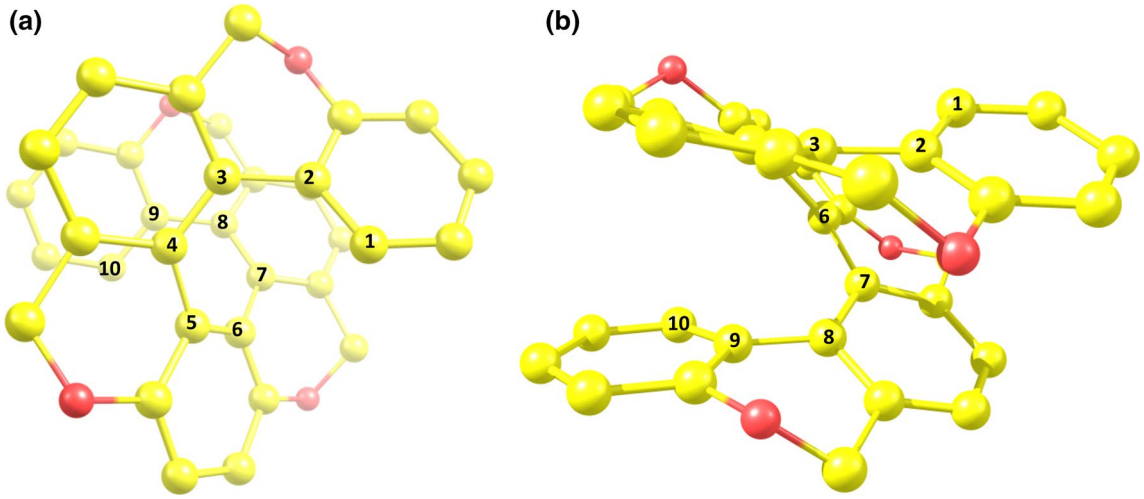

Fig. 4 **a** Top and **b** side view of **1b** with the numbering of the carbons of the inner part. Hydrogens were omitted for clarity. Carbons are in *yellow*, and oxygens in *red*

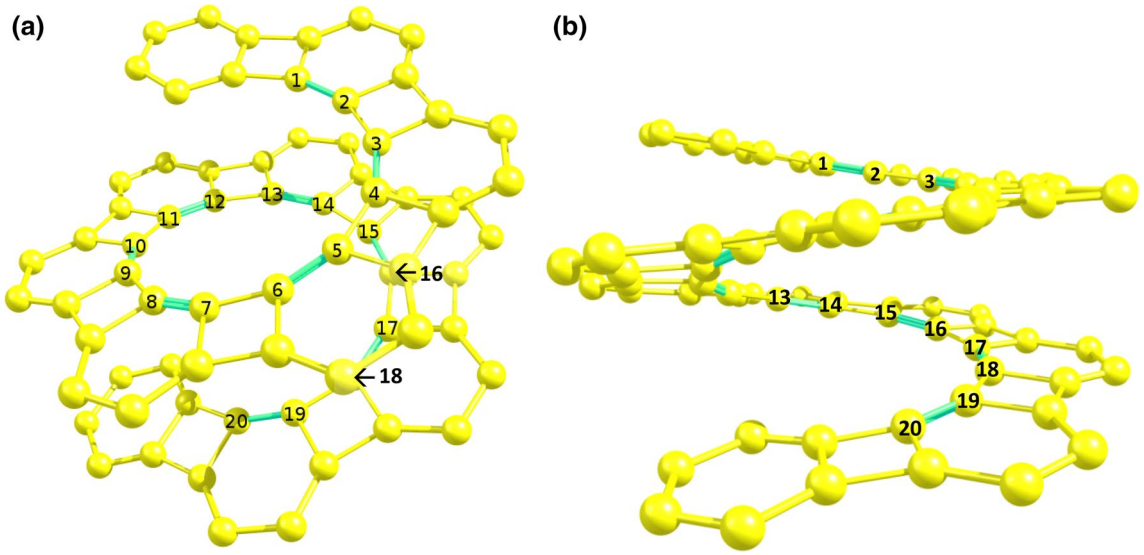

Fig. 5 **a** Top and **b** side view of **2b** with the numbering of the carbons of the inner part. Hydrogens were omitted for clarity. The *green bonds* are shorter than the *yellow ones*, indicating a bond length alternation pattern

single- and double-bond lengths [48]. For a π-conjugation path containing N carbon–carbon bonds, it reads

$$\mathrm{BLA} = \frac{1}{N-1}\sum_{j=1}^{N-1}\left(l_{j+1} - l_j\right)(-1)^j \tag{4}$$

where l_i is the length of bond i. For an aromatic structure, BLA > 0, and for quinonoid ones, BLA < 0 starting with a short bond along the conjugation path. Significant changes in BLA due to oxidation or reduction indicate significant electronic structure changes. We note that due to a relatively large exact exchange contribution in the M05-2X functional, the computed BLA values are expected to be somewhat overestimated [49].

Considering a CT of adding electrons to the lowest unoccupied molecular orbital, LUMO, or removing them from the highest occupied molecular orbital, HOMO, two major effects should be considered. The orbital effect can lead to both positive and negative strain depending on the bonding or antibonding nature of the frontier orbital in

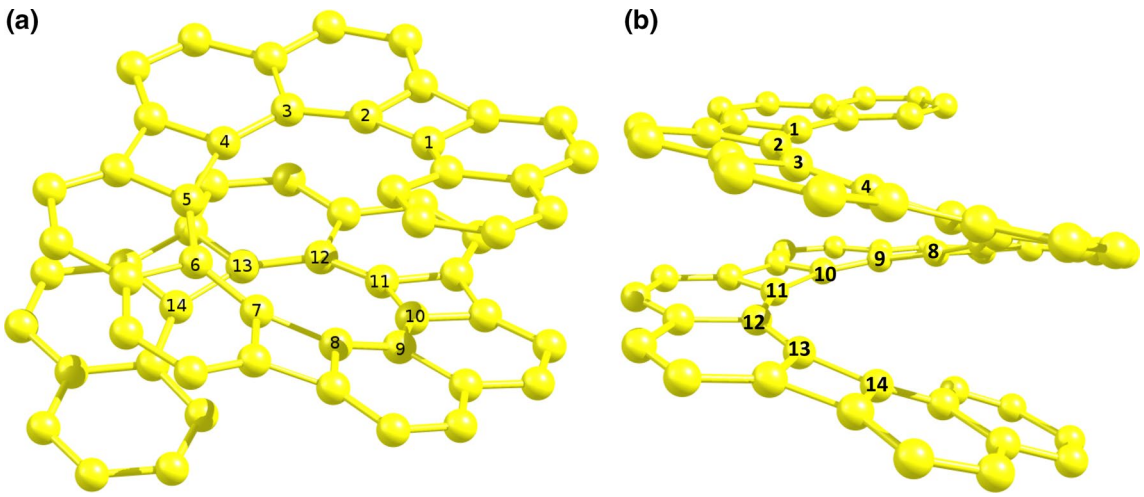

Fig. 6 **a** Top and **b** side view of **3** with the numbering of the carbons in the inner part. Hydrogens were omitted for clarity

Table 1 Index of the carbons (numbering as defined in Figs. 4, 5, and 6) considered in the helix analysis, and total number of carbons included in the average radius, $\bar{r}$

	Index of the carbons	Total number
1b	**1**, 3, 5, 7, **9**	5
2b	**2**, 4, 6, 8, 10, 12, 14, 16, **18**	9
3	**2**, 5, 8, 11, **14**	5

Initial and final carbons for the calculation of Δz are bolded

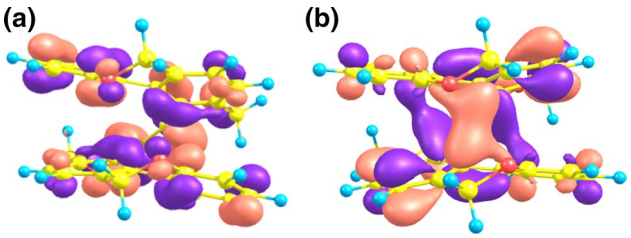

Fig. 7 HOMO of **a 1b** and **b** $\mathbf{1b}^{2-}$. Isosurface was generated with a contour value of 0.030 a.u

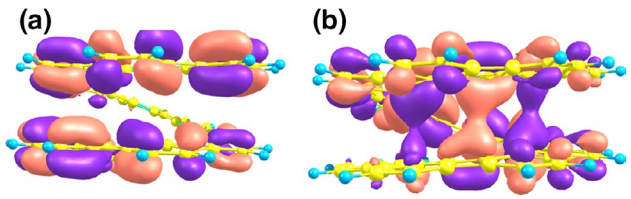

Fig. 8 HOMO of **a 2b** and **b** $\mathbf{2b}^{2-}$. Isosurface was generated with a contour value of 0.021 a.u

question. In addition to the orbital effect, the additional charge is delocalized according to the HOMO or LUMO.

3 Results and discussion

3.1 Changes of the geometry due to CT

All three target molecules show actuation effects upon charging as reflected by the differences of the optimized geometries compared to the $q = 0$ optimized geometry as a reference. One feature of pancake bond is the overlap of the two SOMOs to form mc/2e bonds. Figures 7, 8, 9 show that this is also the case in those molecules when optimized with a modification of the number of electrons. Molecules **1b** and **2b** show this behavior under reduction, while **3** present an overlap for both oxidation and reduction.

Note that the corresponding HOMO–LUMO gaps are large (more than 2.0 eV, see Table S3), while they tend to be small in the case of pancake bonding (Fig. 1). Also, the presence or absence of overlap does not seem to affect the energy levels significantly. As a result, other metrics are to be used for these systems.

3.2 Comparison of the different metrics

Table 2 reports the radius and the average deviation from helicity, using Eq. (3), for each charge state of the 3 molecules. As mentioned, the overlap goes with a shrinking of the distances along the Z axis, as reported in Table 3 for the metric defined in the previous section.

From Table 2, one can see that the CT affects the radius by a few %. Note that the larger radius difference between **2b** and **3** is due to the change from the phenyl units to naphthalenes, and those two molecules have a larger radius than **1b**, due to the presence of unsaturated carbons in

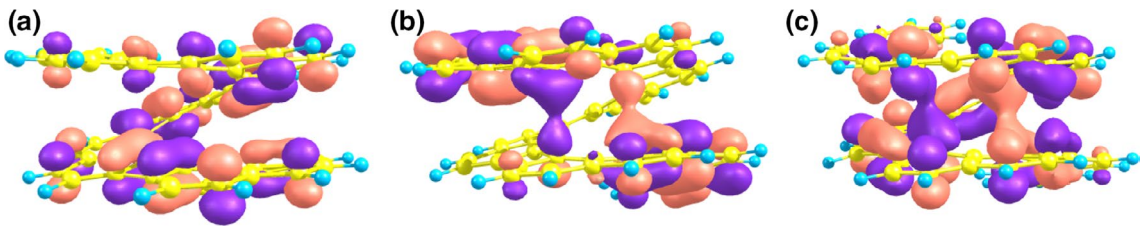

Fig. 9 HOMO of **a 3**, **b** $\mathbf{3^{2+}}$ and **c** $\mathbf{3^{2-}}$. Isosurface was generated with a contour value of 0.030 a.u. for the neutral and oxidized molecule (**a**, **b**), and 0.025 a.u. for the reduced molecule (**c**)

Table 2 Average radius, $\bar{r}$ (Å), and its standard deviation, $\sigma_{\bar{r}}$ (Å), average deviation from helicity, $\bar{D}$ (Å), and its standard deviation, $\sigma_{\bar{D}}$, for **1b**, **2b**, and **3** in different charge states

	Neutral				$q = +2$				$q = -2$			
	$\bar{r}$	$\sigma_{\bar{r}}$	$\bar{D}$	$\sigma_{\bar{D}}$	$\bar{r}$	$\sigma_{\bar{r}}$	$\bar{D}$	$\sigma_{\bar{D}}$	$\bar{r}$	$\sigma_{\bar{r}}$	$\bar{D}$	$\sigma_{\bar{D}}$
1b	1.347	0.040	0.033	0.023	1.345 (−0.2)	0.046	0.042	0.025	1.384 (2.7)	0.038	0.030	0.023
2b	2.903	0.040	0.054	0.027	2.784 (−4.1)	0.174	0.156	0.082	3.120 (7.5)	0.058	0.109	0.062
3	2.189	0.100	0.092	0.049	2.129 (−2.8)	0.100	0.082	0.062	2.011 (−8.1)	0.168	0.165	0.051

For the charged molecules, the percentages of change in the radius from the neutral ones are given in parentheses

Table 3 Changes upon charge transfer of various measures of the molecular length: average pitch, $\bar{p}$ (Å), Δz (Å), and carbon–carbon intramolecular distances, $\overline{d_{CC}}$ (Å), for **1b**, **2b** and **3**

	Neutral			$q = +2$			$q = -2$		
	$\bar{p}$	Δz	$\overline{d_{CC}}$	$\bar{p}$	Δz	$\overline{d_{CC}}$	$\bar{p}$	Δz	$\overline{d_{CC}}$
1b	3.299	4.352	3.378	3.258	4.254	3.334	3.130	4.046	3.182
2b	3.561	4.431	3.688	3.402	4.415[a]	3.884	3.437	3.982	3.500
3	3.308	4.030	3.422	3.148	3.939	3.273	3.246	4.283	3.373

[a] Underlined numbers refer to cases where the helicity is partially lost due to CT (see text)

Table 4 Computed strain due to CT, $s(q)$ (in %), using the three different metrics for **1b**, **2b**, and **3**

	$q = +2$			$q = -2$		
	$s_{\bar{p}}$	$s_{\Delta z}$	$s_{\overline{d_{CC}}}$	$s_{\bar{p}}$	$s_{\Delta z}$	$s_{\overline{d_{CC}}}$
1b	−1.24	−2.25	−1.30	**−5.11**	**−7.02**	**−5.81**
2b	−4.45[b]	−0.35	5.31	**−3.49**	**−10.13**	**−5.09**
3	**−4.82**[a]	**−2.26**	**−4.34**	−1.86	6.28	−1.43

[a] Numbers in bold indicate large actuation (see text)

[b] Underlined numbers indicate partial loss of helicity upon CT (see text)

the latter, which gives more flexibility to the molecule to change its conformation and form the overlap. Under CT, **2b** and **3** undergo a larger change in radius than **1b**. Also, the large standard deviations of the radius for $\mathbf{2b^{2+}}$ and for $\mathbf{3^{2-}}$ (>0.15 Å) indicate that the use of Eq. (2) is more approximate in these cases. This statement is confirmed by the larger average deviations from helicity for those two cases ($\bar{D} > 0.15$ Å).

In Table 3, $\overline{d_{CC}}$ and $\bar{p}$ provide a comparable metric, as expected, but $\overline{d_{CC}}$ is usually larger than $\bar{p}$. The exception is for $\mathbf{2b^{2+}}$ for the reasons mentioned above. It is important to note that in **1b** and **3**, the average pitch is smaller than the carbon–carbon vdW distance (3.4 Å [34]), even for the neutral case. This small through space contact distance is partially responsible for the large actuation effect on the pitch due to CT.

Table 4 lists the strain data for all three systems and both directions of the CT based on Eq. (1) using a subscript to identify which of the three measures of elongation are used. Large strain is obtained for $\mathbf{1b^{2-}}$, $\mathbf{3^{2+}}$, and $\mathbf{2b^{2-}}$. Most of the $s(q)$ values are negative, indicating that the effect is mostly quantum mechanical, and, when negative, in opposition to the Coulombic repulsion due to the extra charge on the molecule. The numbers in bold identify

Table 5 Carbon–carbon intramolecular through space contact distance, d_{CC} (Å), between overlapping carbons (see text for definition) and smallest contact distances for each molecule

	Overlapping carbon number[c]	d_{CC} between overlapping carbons			Smallest d_{CC}		
		Neutral	$q=+2$	$q=-2$	Neutral	$q=+2$	$q=-2$
1b[a]	2···8, 3···9	3.256	3.163, 3.242	**3.030**	3.021	2.975	**2.898**
2b[b]	3···16, (4···17)	3.532	3.822	**3.272**	3.439	3.339	**3.260**
3[b]	2···11, (3···12)	3.188	**3.036**[d]	3.192	3.188	**3.036**	3.137

[a] Due to broken symmetry, two values are given

[b] Due to the C_2 symmetry, only one distance is given (the other pair is given in parentheses)

[c] Carbon numbers refer to Figs. 4, 5, and 6

[d] Numbers in bold indicate large actuation (see text)

Table 6 BLA (Å) for **1b**, **2b** and **3**, calculated by using Eq. (4) for different charge states

	Path definition[a]	BLA		
		Neutral	$q=+2$	$q=-2$
1b	2–9	0.069	0.051	**−0.011**
2b	2–18	0.142	0.136	**0.092**
3	3–6; 6–9; 9–12	0.143	**0.091**[b]	0.089

[a] Carbon numbers refer to Figs. 4, 5, and 6

[b] Bolded numbers indicate the three highest strain systems (see Table 4)

relatively large actuation strains. The number in italics refer to two cases where the helicity is partially lost upon charge transfer, and therefore, the three measures indicate significant discrepancies as we pointed out in connection with the data in Table 4. The large actuation effect is the result of the antibonding nature of the LUMO for **3**, and due to the bonding nature of the HOMO for **1b** and **2b**. The lack of charge symmetry is also apparent as expected for a quantum mechanical mechanism of CT actuation. Molecule $\mathbf{1b^{2-}}$ gives the largest strain values, followed by $\mathbf{3^{2+}}$ and $\mathbf{2b^{2-}}$, if one considers $\bar{p}$ as the measure of the elongation of the molecule. Considering $\overline{d_{CC}}$ confirms that $\mathbf{1b^{2-}}$ is first, but exchanges the order of strains for $\mathbf{3^{2+}}$ and $\mathbf{2b^{2-}}$.

The most significant *through space orbital overlap* is located in the inner part near the C_2 axis of the helix and involves at least four carbons for all three systems, with two pairs of *overlapping carbons* (relation between a pair of overlapping carbon i and j is $\theta_j \approx \theta_i + 360°$, so j is "on top" of i, together with the presence of overlap as shown in Figs. 7, 8, 9). Contact distances are given in Table 5, along with the shortest and/or overlapping contact distances. The values are lower than the average pitch and carbon–carbon distances in Table 4, so one can conclude that local changes are larger than the global changes. Also, except for the reduced $\mathbf{3^{2-}}$, the distances are shorter for the charged molecules with respect to the neutral ones, even if the change is more important when there is an overlap, in comparison with the opposite sign CT (for example, 3.03 Å for $\mathbf{1b^{2-}}$, which present a short contacts with a possibility of a good overlap, vs 3.16 Å for $\mathbf{1b^{2+}}$). Contact distances between overlapping carbons are compatible with the hypothesis of pancake bonds: about 3.00 Å for $\mathbf{1b^{2-}}$ and $\mathbf{3b^{2+}}$ and 3.25 Å for $\mathbf{2b^{2-}}$. The smallest d_{CC} values do not always refer to pairs of overlapping carbons (good overlap would require also the appropriate orientation of the two $2p_z$ atomic orbitals), but short contacts imply that at least one of the four has a good overlap. Therefore, this is the interesting area of the molecule to look at: this is where the actuation is concentrated on.

3.3 Analysis of the molecular strain generated by CT

In Table 6, the BLA values were displayed for both **1b** and **2b**, using Eq. (4) along the path defined by the inner carbons (note that carbons 1 and 10 were omitted in **1b** to start the BLA path with the "short" bond). This analysis is not possible for **3**, because the alternation of single and double bonds is modified by the presence of the naphthalene units. Therefore, another approach was used for **3**: For each 4-membered ring that links two naphthalene units, the inner bond was considered along with its two neighbors, and the average of the length of the two double bonds were subtracted from the length of the single bond. Then, these three values were averaged.

The BLA is lower in the charged systems, so those systems tend to change toward their quinonoid forms, but this decrease in the BLA is more significant if there is an overlap as it is the case for the tree bolded values in Tables 4 and 6 . A BLA change is interpreted as an increase in the π-conjugation, and one can conclude that the form which presents an overlap is more π-conjugated, which is coherent with the large delocalization of the HOMOs in Figs. 7, 8 and 9. For example, a representation of the quinonoid structure of $\mathbf{1b^{2-}}$ is illustrated in Fig. 10.

In Table 7, results from a Mulliken population analysis are given on the respective HOMOs of each three q values, in order to quantify the overlap pictured in Figs. 7, 8, and 9. This sheds light on the participation of the inner part of the structure (see Figs. 4, 5, 6 for the definition) and the 4 atoms that were reported to overlap above in Table 5.

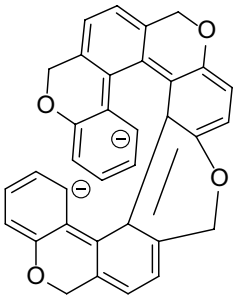

Fig. 10 A representation of the quinonoid structure of $\mathbf{1b}^{2-}$. Distorted metric is used to show the connectivity

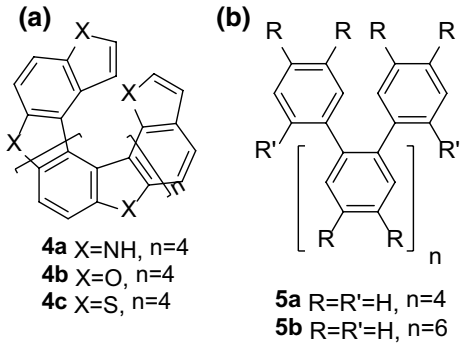

Fig. 11 Alternative helicene-like molecule considered in this work: **a** heterohelicenes (Nakagawa et al. [50] for $n = 3$, X = S) and **b** polymeric *o*-phenylenes (Ohta et al. [39] for $n = 6$, R = OMe and $R' = NO_2$)

This population analysis gives a percentage which is proportional to the presence of the HOMO electrons in a given region of the space. In Table 7, the values for the neutral molecule are low, but when there is CT, a non-negligible part of the population (between 10 and 25 %) is located on the four carbons mentioned in Table 5 in correlation with the presence of an overlap. In that case, the participation of the inner part of the helix accounts for between 38 and 54 % of the population of the orbital. This is in agreement with the previous presented observations as well as the presence of overlaps across the helical pitch as pictured in Figs. 7, 8, and 9.

4 Further systems studied

We have studied (at the same level of theory) five analogous conjugated helical systems with similar architectures which are illustrated in Fig. 11.

Table 8 lists the average deviation from helicity for each systems which is quite large for these systems (larger than in Table 2), making the values difficult to interpret in terms of a helix.

Table 9 gives the calculated strain values using $\bar{p}$, as well as BLA values at different oxidation states. For BLA, the same path definition was used as before: only the inner part of the helix was considered, with the exclusion of the first and the last repeat unit.

The main result from this table is that two systems display large computed actuation values: $\mathbf{4b}^{2+}$ and $\mathbf{5a}^{2-}$. The large positive actuation value for $\mathbf{5a}^{2-}$ indicates that the electrostatic repulsion is not being reduced by an orbital effect which partially explains the actuation in this case. The significant negative actuation value for $\mathbf{4b}^{2+}$ is in concordance with strong bonding interaction displayed in Fig. 12. Except for this case, structures **4** and **5** miss an overlap in their frontier orbitals with CT.

While we did not find one general reason for the lack of orbital overlap-based charge transfer actuation for the molecules in Fig. 11, a pattern arises: Heteroatoms (for example sulfur) on the periphery in **4** tend to have X···X contacts larger than vdW distances, and for this reason, the overlap across the pitch is small. In the case of **5**, the actuation reported by Ohta et al. [39] via oxidation is confirmed by our calculations (**5b**), but this is probably due to a reduction in the length of inter-phenyl bond lengths, as shown by the reduction in the BLA value. Note that the large positive strain value for $\mathbf{5a}^{2-}$ is partially related to the large deviation from the helical structure (as shown in Table 8, with $\bar{D} > 0.90$ Å), probably due to the presence of less phenyl rings to constrain the structure. Concerning $\mathbf{4b}^{2+}$, the strain is negative, but the large $\bar{D} = 0.14$ Å value for **4b** indicates a large deviation from helicity. Also, the pitch

Table 7 Percentage of the HOMO localized on the 4 carbons that present a direct overlap ("4 carbons" as defined in Table 5) and localized on the inner part of the helix ("Inner part" as defined in Figs. 4, 5, 6) for molecules **1b**, **2b**, and **3**, using a Mulliken population analysis

	Neutral		$q = +2$		$q = -2$	
	4 carbons	Inner part	4 carbons	Inner part	4 carbons	Inner part
1b	7(2)	26 (10)	11 (2)	20 (5)	**16 (4)**	**48 (10)**
2b	0 (0)	1 (1)	0 (0)	4 (1)	**10 (4)**	**54 (18)**
3	6 (2)	34 (10)	**22 (4)**[a]	**38 (7)**	14 (4)	30 (10)

The number of carbons involved in this percentage is given in parentheses

[a] Bolded numbers refer to the three highest strain systems

Table 8 Average deviation from helicity, $\bar{D}$ (Å), and its standard deviation, $\sigma_{\bar{D}}$, for **4a–c**, and **5a**–**b** in different charge states

	Neutral		$q = +2$		$q = -2$	
	$\bar{D}$	$\sigma_{\bar{D}}$	$\bar{D}$	$\sigma_{\bar{D}}$	$\bar{D}$	$\sigma_{\bar{D}}$
4a	0.122	0.066	0.107	0.053	0.107	0.055
4b	0.140	0.068	0.090	0.039	0.106	0.039
4c	0.125	0.051	0.112	0.045	0.127	0.055
5a	0.350	0.042	0.441	0.063	0.914	0.144
5b	0.051	0.022	0.077	0.039	0.122	0.024

Table 9 Strain values due to CT $[s_{\bar{p}}(q)$ in %$]$ and bond length alternation (BLA, in Å) for **4a**–**4c** and **5a**–**5b** for different charge states

	$s_{\bar{p}}$		BLA		
	$q = +2$	$q = -2$	Neutral	$q = +2$	$q = -2$
4a	0.09	0.20	0.029	0.047	−0.005
4b	**−7.34**[a]	−2.85	0.040	0.005	−0.008
4c	−0.89	1.07	0.034	0.023	−0.011
5a	−1.95[b]	**14.77**	0.082	0.040	0.043
5b	−2.74	3.52	0.082	0.051	0.049

[a] Numbers in bold indicate large actuation (see text)

[b] Underlined numbers indicate partial loss of helicity upon CT (based on the values in Table 8, see text)

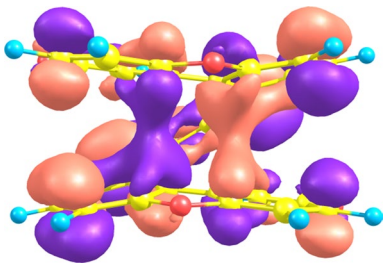

Fig. 12 HOMO of $\mathbf{4b}^{2+}$ (isosurface was generated with a contour value of 0.021 a.u.)

as measured by $\bar{p}$ is 3.24 Å for $\mathbf{4b}^{2+}$, which is larger than $\mathbf{3}^{2+}$ and $\mathbf{1b}^{2-}$ (<3.2 Å, see Table 3) presented before. This partially explains why the effect of the overlap is smaller in this case.

5 Conclusions

In this paper, we discussed the charge transfer actuation mechanism in helical conjugated molecules. We find significant actuation values for molecules with repeat units that appear to be synthesizable.

Molecules **1b** and **2b** present a large strain under reduction, while a large strain is obtained under oxidation for **3**. This change of the number of electrons is accompanied with a modification of the radius of the molecule. We discussed three alternative measures for strain in a helix pointing out the limitations of these metrics when the structure deviates from an exactly helical shape. The strains are significant and larger than 5 % with two electrons added or removed, which is comparable to other values in the literature.

The shrinking generated by CT is accompanied by a large modification of the BLA, with a clear shift toward a quinonoid structure. The strain caused by CT is strongly correlated with the presence of an across the pitch overlap in the relevant frontier orbital. This overlap is concentrated in the inner parts of the molecules.

In the oxidized or reduced systems, there are some hints of the presence of a pancake bonding, but there are some significant differences. First, the structure presents no spin densities when there is an overlap. It was also mentioned that the HOMO–LUMO gaps are large in these systems, which is generally not the case with pancake bonds. Therefore, what is observed for **1b**, **2b**, and **3** should be more thought of as a *through space* interactions rather than pancake bonds.

$\mathbf{4b}^{2+}$ and $\mathbf{5a}^{2-}$ also show large actuation values. While the mechanisms vary, the presented examples indicate that various helical molecules should show electromechanical actuation effects similar to the ones described in this paper and that the order of this effect should be several percent strain per electron transferred.

Acknowledgments P. B. is grateful to the *Fond d'aide à la mobilité étudiante* (FAME) for a FAME/BMI traineeships grant and a Visiting Scientist Fellowship to Georgetown University. We thank the U S National Science Foundation for its support of this research at Georgetown University (Grant Number CHE-1006702). MK is member of the Georgetown Institute of Soft Matter.

References

1. Baughman RH (2005) Science 308:63–65
2. Mirfakhrai T, Madden JDW, Baughman RH (2007) Mater Today 10:30–38
3. Göpel W (1991) Sens Actuators B Chem 4:7–21

4. Smela E (2003) Adv Mater 15:481–494
5. Terao F, Morimoto M, Irle M (2012) Angew Chem Int Ed 51:901–904
6. Ebron VH, Yang Z, Seyer DJ, Kozlov ME, Oh J, Xie H, Razal J, Hall LJ, Ferraris JP, MacDiarmid AG, Baughman RH (2006) Science 311:1580–1583
7. Yu HH, Swager TM (2004) IEEE J Ocean Eng 29:692–695
8. Marsella MJ, Reid RJ (1999) Macromolecules 32:5982–5984
9. Barboiu M, Vaughan G, Kyritsakas N, Lehn JM (2003) Chem Eur J 9:763–769
10. Juluri BK, Kumar AS, Liu Y, Ye T, Yang YW, Flood AH, Fang L, Stoddart JF, Weiss PS, Huang TJ (2009) ACS Nano 3:291–300
11. Huang TJ, Brough B, Ho C-M, Liu Y, Flood AH, Bonvallet PA, Tseng H-R, Stoddart JF, Baller M, Magonov S (2004) Appl Phys Lett 85:5391
12. Madden JD, Cush RA, Kanigan TS, Brenan CJ, Hunter IW (1999) Synth Met 105:61–64
13. Madden JD, Cush RA, Kanigan TS, Hunter IW (2000) Synth Met 113:185–192
14. Qi B, Lu W, Mattes BR (2004) J Phys Chem B 108:6222–6227
15. Tahhan M, Truong V-T, Spinks GM, Wallace GG (2003) Smart Mater Struct 12:626–632
16. Han G, Shi G (2004) Sens Actuators B Chem 99:525–531
17. Baughman RH (1999) Science 284(80):1340–1344
18. Bissell RA, Córdova E, Kaifer AE, Stoddart JF (1994) Nature 369:133–137
19. Credi A, Balzani V, Langford SJ, Stoddart JF (1997) J Am Chem Soc 119:2679–2681
20. Tseng HR, Vignon SA, Stoddart JF (2003) Angew Chem Int Ed 42:1491–1495
21. Badjic JD, Balzani V, Credi A, Silvi S, Stoddart JF (2004) Science 303:1845–1849
22. Tian YH, Kertesz M (2009) Chem Mater 21:2149–2157
23. Song C, Swager TM (2008) Org Lett 10:3575–3578
24. Chebny VJ, Shukla R, Lindeman SV, Rathore R (2009) Org Lett 11:1939–1942
25. Scherlis DA, Marzari N (2005) J Am Chem Soc 127:3207–3212
26. Goto K, Kubo T, Yamamoto K, Nakasuji K, Sato K, Shiomi D, Takui T, Kubota M, Kobayashi T, Yakusi K, Ouyang JY (1999) J Am Chem Soc 121:1619–1620
27. Zheng SJ, Lan J, Khan SI, Rubin Y (2003) J Am Chem Soc 125:5786–5791
28. Small D, Rosokha SV, Kochi JK, Head-Gordon M (2005) J Phys Chem A 109:11261–11267
29. Zaitsev V, Rosokha SV, Head-Gordon M, Kochi JK (2006) J Org Chem 71:520–526
30. Haddon RC (2012) ChemPhysChem 13:3581–3583
31. Suzuki S, Morita Y, Fukui K, Sato K, Shiomi D, Takui T, Nakasuji K (2006) J Am Chem Soc 128:2530–2531
32. Tian YH, Kertesz M (2010) J Am Chem Soc 132(31):10648–10649
33. Cui ZH, Lischka H, Beneberu HZ, Kertesz M (2014) J Am Chem Soc 136:5539–5542
34. Bondi A (1964) J Phys Chem 68:441–451
35. Mou Z, Uchida K, Kubo T, Kertesz M (2014) J Am Chem Soc 136:18009–18022
36. Rempala P, King BT (2006) J Chem Theory Comput 2:1112–1118
37. Mathew SM, Hartley CS (2011) Macromolecules 44:8425–8432
38. Mathew SM, Engle JT, Ziegler CJ, Hartley CS (2013) J Am Chem Soc 135:6714–6722
39. Ohta E, Sato H, Ando S, Kosaka A, Fukushima T, Hashizume D, Yamasaki M, Hasegawa K, Muraoka A, Ushiyama H, Yamashita K, Aida T (2011) Nat Chem 3:68–73
40. Kimura Y, Fukawa N, Miyauchi Y, Noguchi K, Tanaka K (2014) Angew Chem Int Ed 53:8480–8483
41. Han S, Bond AD, Disch RL, Holmes D, Schulman JM, Teat SJ, Vollhardt KPC, Whitener GD (2002) Angew Chem Int Ed 114:3357–3361
42. Sun G, Kürti J, Kertesz M, Baughman RH (2002) J Am Chem Soc 124:15076–15080
43. Zhao Y, Schultz EN, Truhlar DG (2006) J Chem Theory Comput 2:364–382
44. Beneberu HZ, Tian TH, Kertesz M (2012) Phys Chem Chem Phys 14:10713–10725
45. Frisch MJ et al (2013) Gaussian 09, Revision D.01. Gaussian Inc., Wallingford
46. Zhurko GA, Zhurko DA Chemcraft, Version 1.8 (2015). http://Chemcraftprog.com
47. Helix, in Wolfram Mathworld. http://mathworld.wolfram.com/Helix.html. Accessed on 13 May 2015
48. Longuet-Higgins HC, Salem L (1959) Proc R Soc A Math Phys Eng Sci 251:172–185
49. Kertesz M, Choi CH, Yang SJ (2005) Chem Rev 105:3448–3481
50. Nakagawa H, Yoshino J, Yamada K, Shiro M (2003) Chem Lett 32:90–91